Quasi-Fluid-Mechanics-Based Quasi-Bayesian Cramér–Rao Bounds for Deformed Towed-Array Direction Finding

Petr Tichavský, *Member, IEEE,* and Kainam Thomas Wong, *Senior Member, IEEE*

***Abstract*—New quasi-Bayesian (hybrid) Cramér-Rao bound (CRB) expressions are herein derived for far-field deep-sea direction-of-arrival (DOA) estimation with a nominally linear towed-array that 1) is deformed by *spatio-temporally correlated* oceanic currents, which have been previously overlooked in the towed-array shape-deformation statistical analysis literature, 2) is deformed by *temporally correlated* motion of the towing vessel, which is modeled only as temporally *un*correlated in prior literature, and 3) suffers gain-uncertainties and phase-uncertainties in its constituent hydrophones. This paper attempts to bridge an existing literature gap in deformed towed-array DOA-estimation performance analysis, by *simultaneously* a) incorporating several essential fluid-mechanics considerations to produce a shape-deformation statistical model physically more realistic than those previously used for DOA performance analysis and b) rigorously derive a mathematical analysis to characterize quantitatively and qualitatively the DOA stimation's statistical performance. The derived CRB expressions are parameterized in terms of the towed-array's physically measurable nonidealities for the single-source case. The new hybrid-CRB expressions herein derived are numerically more stable than those in the current literature.**

***Index Terms*—Acoustical signal processing, array signal processing, direction-of-arrival estimation, marine telemetry, parameter estimation, sonar arrays, sonar signal processing, underwater acoustic arrays.**

I. Introduction

A towed-array consists of an acoustically transparent and neutrally buoyant cable of hydrophones hauled behind a surface ship or a submerged vessel. A towed array may extend for several tens of meters to several hundreds of meters. The towed array's nominally linear geometry may be arbitrarily distorted by the towing vessel's varying speed and transverse motion, by the array's non-neutral buoyance and nonuniform changes in density, and by hydrodynamic effects plus oceanic swells and currents. The resulting snake-like deformation from the array's nominal linearity can lead to critical degradation in the accuracy of arrival angle estimation/tracking, beamforming, and imaging because all these signal processing operations are predicated on a sufficiently accurate (*a priori* or estimated) model of the array's inter-hydrophone spacings.

Towed-array deformity has been investigated by researchers from several complementary perspectives: Towed arrays' geometric deformation has been empirically measured [13], [24], [35], computer simulated [39], and theoretically predicted based on fluid mechanics and oceanic physics [1]–[3], [7], [8], [11], [12]. A wealth of array-shape calibration algorithms have been devised using cooperative sources from known arrival-angles (in "aided calibration") [23], [34], [38], by exploiting noncooperative sources from unknown arrival angles (in "self-calibration") [9], [10], [14], [18], [22], [25], [29], [36], or by attaching on the towed-array nonacoustic positioning-devices (such as heading-sensors, depth-sensors and compasses to estimate the array's displacements along the array-length axis, the vertical transverse axis and the horizontal transverse axis, respectively) [8], [16], [21], [24], [27]. The present work provides a quantitative analysis of bearing-estimation accuracy for deformed towed-arrays, assuming array shape-deformation information is available from neither cooperative calibration sources nor from nonacoustic positioning devices.

A. Literature on Modeling Towed-Array Shape-Deformation

The towed-array shape-deformation modeling literature generally falls into two categories: 1) fluid-mechanics-intensive models that are physically accurate but mathematically intractable for statistical signal parameter-estimation performance analysis and (2) mathematically simple models that overlooks most (if not all) fluid-mechanics-based considerations. The present manuscript aims to make one *initial* step toward bridging this crucial literature gap between 1) and 2) above by incorporating certain (admittedly, not all) essential fluid-mechanics considerations into the statistical measurement model, while drawing out in detail with rigorous mathematics a comprehensive (admittedly, not exhaustive) analysis of what this enhanced model implies in the statistical performance of direction-of-arrival (DOA) estimation.

1) Fluid-Mechanics-Intensive Models: Transverse deformation/vibration of a thin flexible cylinder, towed by a vessel, has been shown to obey a fourth-order partial differential equation known as the Paidoussis equation [1]–[3], [11], [12]. This equation, which was first applied in the towed-array

Manuscript received December 30, 2002; revised April 4, 2003. Part of this paper was presented at the 2002 IEEE International Conference on Acoustics, Speech, and Signal Processing, Orlando, FL. P. Tichavský was supported by the Grant Agency of the Czech Republic through Grant 102/01/0021. K. T. Wong was supported by Canada's Natural Sciences and Engineering Research Council's Individual Research Grant NSERC-RGPIN-249775-02. The associate editor coordinating the review of this paper and approving it for publication was Dr. Alex B. Gershamn.

P. Tichavský is with the Institute of Information Theory and Automation, the Academy of Sciences of the Czech Republic, Prague, Czech Republic (e-mail: p.tichavsky@ieee.org).

K. T. Wong is with the Department of Electrical and Computer Engineering, University of Waterloo, Waterloo, ON N2L 3G1, Canada (e-mail: ktwong@ieee.org).

Digital Object Identifier 10.1109/TSP.2003.820072

context in [7] and [8], describes the mechanical propagation of array-deformation down the array's length. The validity of this theoretical model was verified under field conditions [2].

Fluid-mechanics-based array deformation models have been used to investigate only array shape calibration in [21], [24], [36], and [38] but not for the present objective of DOA-estimation Cramér-Rao bound (CRB) analysis. Moreover, these models from [21], [24], [36], and [38] overlook the oceanic currents' statistical influence in the Paidoussis equation on array shape deformation. These earlier works also model the towing vessel's movement as temporally *un*correlated, which may be physically unrealistic for high time-sampling rates. In contrast, the present analysis offers more realism by allowing arbitrary temporal correlation (while assuming statistical stationarity) in the towing vessel's motion.

2) Mathematically Simple Models With Little Fluid Mechanics: A wealth of CRB analysis exists in the antenna-array signal-processing research literature on DOA estimation with uncertainties in the inter-antenna spacings. However, this antenna-array literature presumes *spatially*[1] *un*correlated and *spatially stationary* locational uncertainties from sensor to sensor. Unfortunately, such assumptions are manifestly invalid for a towed array, whose elements are strung up on a cable. Spatial *decorrelation*, in the towed array context, would imply rather implausibly that an upstream hydrophone's positional deviation has no effect on the downstream hydrophones' positional deviations. Spatial *stationarity* would unrealistically imply that the hydrophone secured at the tow point likely has a positional deviation comparable with those hydrophones at the tow cable's unsecured free end.

Among all DOA estimation CRB work accounting for spatial correlation among the sensors' dislocation (see [4], [5], [9], [10], [14], [17], [18], [20], [25], [26], [28], [29], [40]), none uses an array-deformation model rigorously derived from fluid mechanics. *Ad hoc* statistical models for array-shape deformation include [4], [9], [10], and [17], which assume as statistically *un*correlated the transverse and array-length axis positional perturbations. In [4], the transverse perturbations to be spatially correlated from hydrophone to hydrophone with a dependence inversely exponential to the cable length connecting the two hydrophones, but without rigorous justification, are modeled. In [9] and [10], the prior distribution for both the transverse uncertainties and the array-length axis uncertainties is assumed to be spatially uncorrelated Gaussian, which is an assumption that unrealistically implies that hydrophones near the tow point have positional variances comparable with those at the cable's free end. The rudimentary model of [17] postulates nothing beyond the aforementioned uncorrelated condition between the transverse and array-length axis positional perturbations. Another *ad hoc* deformation model is used in [28], without any physics-based justification, involving a transverse perturbation whose standard deviation increases quadratically downstream and a linearly increasing perturbation along the array-length axis. The spatial correlation and the transverse/array-length correlation in [28] are both 100% correlated.

The more sophisticated deterministic piecewise-linear model presumes the relative angles between adjoining piecewise-linear segments to be deterministic unknown constants. For example, [22], [23], [29], [33], [34], and [38] use the deterministic piecewise linear shape deformation model for array shape calibration performance analysis. A stochastic piecewise-linear model, assuming the relative angle between adjoining piecewise-linear segments to be Gaussian and (implausibly[2] as) spatially uncorrelated, is used in [29] for DOA estimation.

Moreover, much of the above-mentioned deformed-array bearing-estimation literature (all except [17], [28], and [29] and unlike the present work) unrealistically assumes that no uncertainty exists in the hydrophone's gain and phase responses. This work attempts to be comprehensive in accounting simultaneously for diverse array nonidealities.

B. CRB Literature on Deformed-Array DOA Estimation

The DOA estimation lower bounds herein derived are quasi-Bayesian (hybrid) CRBs that characterize the best standard deviation obtainable using any unbiased estimator of a vector parameter. The CRB may serve as a performance metric in towed-array design with any required level of bearing estimation accuracy.

The terms "quasi-Bayesian" and "hybrid" aim to contrast against the standard CRB to signify that the vector-parameter here has a deterministic subvector and a random nuisance-parameter subvector. The former consists of the incident sources' unknown but to-be-estimated angles of arrival. The latter does not need to be estimated but characterizes the array-shape deformations, the phase/gain uncertainties of the individual acoustic sensors, and other factors. The "hybrid" (quasi-Bayesian) CRB may be defined as a proper submatrix of the overall vector-parameter's CRB matrix, which is equal to the inverse of the corresponding Fisher information matrix. The bound depends on the *a priori* distribution (uncertainty) of the random subvector. It depends only on the signal/noise statistical model but not the particular estimation algorithm method used; however, the quasi-Bayesian CRB may be attained by an maximum *a posteriori* (MAP) estimator of the parameter-estimation problem [29].

The present analysis allows a broad class of Bayesian-like statistical models parameterized with physically measurable quantities. For example, certain independent parameters [describing the tow-point induced (TPI) motion and oceanic currents] in the Paidoussis equation are herein characterized as stochastic with known prior distributions instead of as deterministic unknowns. This quasi-Bayesian approach is advantageous because the underlying fluid mechanical and oceanic physical processes (that cause the array's geometric deformation) can be neither exactly measured nor precisely estimated. Hence, they would best be modeled as stochastic phenomena. As oceanic engineers gather new data and update the statistics of such TPI-motion and oceanic current, the statistical properties of the Bayesian parameters may be estimated and substituted in the CRB formulas presented in this paper. Lower bounds of the deformed towed-array's DOA-estimation variance can then be obtained along with the general expressions for the quasi-Bayesian Cramér-Rao lower bound, which is derived in [29]. Among all prior work cited in the preceding paragraphs, only [4], [9], [10], [17], [28],

[1]"Space" as spanned by the array's geometrical axes.

[2]See further discussion in the following paragraphs.

and [29] also use a Bayesian approach, but (as discussed in the preceding subsection) none of these papers model array shape deformation based on rigorous fluid mechanics, as in the present work.

This paper is partly based on the generic CRB expression derived in [29] for sensor-array estimation under array uncertainties. Because this expression might be numerically unstable when the data-length N approaches infinity or when the covariance matrices of array dislocations are small, this present paper derives an alternative expression that is numerically more stable. This new expression allows easy computation of the limit-CRB for N approaching infinity. As an example, the CRB is herein computed in the case of a single source. The main contribution of the paper, however, consists of computing physically meaningful covariance matrices of array dislocations, which was discussed in the previous subsection.

II. Mathematical Data Models for Far-Field Sources Propagating Through a Deep-Sea Channel

This section introduces the mathematical and statistical data models involved in far-field deep-sea direction finding. K far-field narrowband sources impinge on an L-hydrophone array as plane waves without time-delayed multipaths to produce at time t the measured data vector:

$$\mathbf{d}(t) = \mathbf{A}(\boldsymbol{\theta}, \boldsymbol{\rho})\, \mathbf{s}(t) + \mathbf{n}(t). \tag{1}$$

The kth column $\mathbf{a}_k(\boldsymbol{\theta}, \boldsymbol{\rho})$ of the $L \times K$ matrix $\mathbf{A}(\boldsymbol{\theta}, \boldsymbol{\rho})$ represents the kth source's steering vector, which has as components[3]

$$[\mathbf{a}_k(\boldsymbol{\theta}, \boldsymbol{\rho})]_\ell = g_\ell\, e^{j\varphi_\ell}\, e^{j2\pi(x_\ell u_k + y_\ell v_k + z_\ell w_k)/\lambda}, \quad \ell = 1, \ldots, L \tag{2}$$

where (u_k, v_k, w_k) represent the Cartesian direction-cosines of the kth incident source, g_ℓ and φ_ℓ, respectively, denote the ℓth sensor's unity-mean gain-perturbation and zero-mean phase-perturbation, (x_ℓ, y_ℓ, z_ℓ) symbolize the three-dimensional (3-D) Cartesian position coordinates of the ℓth sensor, and λ denotes the wavelength. The kth element in the $K \times 1$ vector $\mathbf{s}(t)$ represents the kth frequency-down-converted incident temporal signal and is modeled as a temporally uncorrelated zero-mean complex-valued circular-Gaussian stochastic process with $\mathbf{s}(t)$ having the *a priori* unknown covariance matrix $\boldsymbol{\Omega}_\mathbf{s}$. The lth element in the $L \times 1$ vector $\mathbf{n}(t)$ refers to the spatio-temporally uncorrelated complex-valued additive noise at the lth hydrophone, with *a priori* unknown variance σ^2.

The $M_{\boldsymbol{\theta}} \times 1$ vector $\boldsymbol{\theta}$ contains as its elements the to-be-estimated unknown deterministic signal parameters, e.g., the azimuth and/or elevation angles or, equivalently, the Cartesian direction cosines. The $M_{\boldsymbol{\rho}} \times 1$ nuisance vector $\boldsymbol{\rho}$ consists of the nuisance parameters — $\{g_\ell, \varphi_\ell, x_\ell, y_\ell, z_\ell,\ \ell = 1, \ldots, L\}$. Further, define $\mathbf{g} = [g_1, \ldots, g_L]^T$, $\boldsymbol{\varphi} = [\varphi_1, \ldots, \varphi_L]^T$, $\mathbf{x} = [x_1, \ldots, x_L]^T$, $\mathbf{y} = [y_1, \ldots, y_L]^T$, and $\mathbf{z} = [z_1, \ldots, z_L]^T$. These stochastic parameter vectors are modeled as mutually independent and real-valued Gaussian distributed, with *a priori* known nominal means $\mathbf{g}_0$, $\boldsymbol{\varphi}_0$, $\mathbf{x}_0$, $\mathbf{y}_0$, $\mathbf{z}_0$, and *a priori* known covariance matrices $\boldsymbol{\Omega}_{\Delta g}$, $\boldsymbol{\Omega}_{\Delta\varphi}$, $\boldsymbol{\Omega}_{\Delta x}$, $\boldsymbol{\Omega}_{\Delta y}$, and $\boldsymbol{\Omega}_{\Delta z}$. Hence, $\boldsymbol{\rho}$ may be represented as a real-valued, Gaussian, stochastic vector with *a priori* known mean $\boldsymbol{\rho}_0$ and *a priori* known covariance matrix $\boldsymbol{\Omega}_{\boldsymbol{\rho}}$. To summarize, the present data model involves the unknown *stochastic* entities of $\boldsymbol{\rho}$, $\mathbf{s}(t)$ and $\mathbf{n}(t)$, plus the unknown *deterministic* entities of $\boldsymbol{\theta}$, $\boldsymbol{\Omega}_\mathbf{s}$, and σ^2. However, only $\boldsymbol{\theta}$ needs to be estimated.

[3]The index k will be dropped in the case of a single source.

III. New CRB Expression Compatible with Various To-Be-Specified Quasi-Bayesian Models of Array Nonidealities

In [29], there is a "generic" quasi-Bayesian CRB expression applicable to far-field deep-sea nonideal array direction finding. Building on [29], this section will develop CRB expressions that 1) are numerically more stable and applicable to any number of incident sources, 2) reveal the multisource CRBs asymptotic behavior as the data-length N approaches infinity, and 3) link to the physical quantities parameterizing various array nonidealities in the single-source case. From [29]:

$$\begin{aligned}\mathrm{E}[(\hat{\boldsymbol{\theta}} - \boldsymbol{\theta}_0)(\hat{\boldsymbol{\theta}} - \boldsymbol{\theta}_0)^T] \geq & \mathrm{CRB}_{\boldsymbol{\theta}} \\ = & \frac{1}{N}[\mathbf{C}_{\boldsymbol{\theta}\boldsymbol{\theta}} - \mathbf{C}_{\boldsymbol{\rho}\boldsymbol{\theta}}^T(\mathbf{C}_{\boldsymbol{\rho}\boldsymbol{\rho}} + (2N\boldsymbol{\Omega}_{\boldsymbol{\rho}})^{-1})^{-1}\mathbf{C}_{\boldsymbol{\rho}\boldsymbol{\theta}}]^{-1}\end{aligned} \tag{3}$$

where

$$\mathbf{C}_{\boldsymbol{\theta}\boldsymbol{\theta}} = \mathrm{Re}\{\mathbf{D}_{\boldsymbol{\theta}}^H\, \mathbf{M}\, \mathbf{D}_{\boldsymbol{\theta}}\}$$
(real-valued, $M_\theta \times M_\theta$ in size) (4)

$$\mathbf{C}_{\boldsymbol{\rho}\boldsymbol{\theta}} = \mathrm{Re}\{\mathbf{D}_{\boldsymbol{\rho}}^H\, \mathbf{M}\, \mathbf{D}_{\boldsymbol{\theta}}\}$$
(real-valued, $M_\rho \times M_\theta$ in size) (5)

$$\mathbf{C}_{\boldsymbol{\rho}\boldsymbol{\rho}} = \mathrm{Re}\{\mathbf{D}_{\boldsymbol{\rho}}^H\, \mathbf{M}\, \mathbf{D}_{\boldsymbol{\rho}}\}$$
(real-valued, $M_\rho \times M_\rho$ in size) (6)

$$\mathbf{D}_{\boldsymbol{\theta}} = \left[\frac{\partial \mathrm{vec}\,[\mathbf{A}(\boldsymbol{\theta}, \boldsymbol{\rho})]}{\partial \boldsymbol{\theta}_1}, \ldots, \frac{\partial \mathrm{vec}\,[\mathbf{A}(\boldsymbol{\theta}, \boldsymbol{\rho})]}{\partial \boldsymbol{\theta}_{M_{\boldsymbol{\theta}}}}\right]$$
(complex-valued, $LK \times M_\theta$ in size) (7)

$$\mathbf{D}_{\boldsymbol{\rho}} = \left[\frac{\partial \mathrm{vec}\,[\mathbf{A}(\boldsymbol{\theta}, \boldsymbol{\rho})]}{\partial \boldsymbol{\rho}_1}, \ldots, \frac{\partial \mathrm{vec}\,[\mathbf{A}(\boldsymbol{\theta}, \boldsymbol{\rho})]}{\partial \boldsymbol{\rho}_{M_{\boldsymbol{\rho}}}}\right]$$
(complex-valued, $LK \times M_\rho$ in size) (8)

$$\mathbf{M} = \sigma^{-2}\{\boldsymbol{\Omega}_\mathbf{s}\mathbf{A}^H(\boldsymbol{\theta}_0, \boldsymbol{\rho}_0)\mathbf{R}^{-1}\mathbf{A}(\boldsymbol{\theta}_0, \boldsymbol{\rho}_0)\boldsymbol{\Omega}_\mathbf{s}\}^T \otimes \boldsymbol{\Pi}_A^\perp$$
(complex-valued, $LK \times LK$ in size) (9)

$$\mathbf{R} = \mathbf{A}(\boldsymbol{\theta}_0, \boldsymbol{\rho}_0)\boldsymbol{\Omega}_\mathbf{s}\mathbf{A}^H(\boldsymbol{\theta}_0, \boldsymbol{\rho}_0) + \sigma^2\mathbf{I}$$
(complex-valued, $L \times L$ in size) (10)

$$\boldsymbol{\Pi}_A^\perp = \mathbf{I} - \mathbf{A}(\boldsymbol{\theta}_0, \boldsymbol{\rho}_0)(\mathbf{A}(\boldsymbol{\theta}_0, \boldsymbol{\rho}_0)^H\mathbf{A}(\boldsymbol{\theta}_0, \boldsymbol{\rho}_0))^{-1}\mathbf{A}(\boldsymbol{\theta}_0, \boldsymbol{\rho}_0)^H$$
(complex-valued, $L \times L$ in size) (11)

where $\otimes$ denotes the Kronecker product, $\boldsymbol{\theta}_0$ represents the theoretical value of $\boldsymbol{\theta}$, and the derivatives in (7) and (8) are evaluated for $\boldsymbol{\theta} = \boldsymbol{\theta}_0$ and $\boldsymbol{\rho} = \boldsymbol{\rho}_0$.

The $\mathrm{CRB}_{\boldsymbol{\theta}}$ expression in (3) might be numerically unstable because $\boldsymbol{\Pi}_A^\perp$ is rank-deficient, as $\boldsymbol{\Pi}_A^\perp$ represents a projection operator such that $\boldsymbol{\Pi}_A^\perp\mathbf{A}(\boldsymbol{\theta}_0, \boldsymbol{\rho}_0) = \mathbf{0}$. This means that $\mathbf{C}_{\boldsymbol{\rho}\boldsymbol{\rho}}$ and $\mathbf{M}$ are both rank-deficient, and consequently, the to-be-inverted term $\mathbf{C}_{\boldsymbol{\rho}\boldsymbol{\rho}} + (2N\boldsymbol{\Omega}_{\boldsymbol{\rho}})^{-1}$ might be ill-conditioned for large $N\boldsymbol{\Omega}_{\boldsymbol{\rho}}$.

Assume that $\mathbf{A}$ has full column rank. Then, the projection operator $\mathbf{\Pi}_A^{\perp}$ has rank $L-K$ and

$$\mathbf{\Pi}_A^{\perp} = \mathbf{B}(\mathbf{B}^H\mathbf{B})^{-1}\mathbf{B}^H \tag{12}$$

where $\mathbf{B}$ consists of the $L-K$ linearly independent columns of $\mathbf{\Pi}_A^{\perp}$ that span the column space of $\mathbf{\Pi}_A^{\perp}$. Usually, $\mathbf{B}$ can be formed from the first $L-K$ columns of $\mathbf{\Pi}_A^{\perp}$, i.e., $\mathbf{B} = \mathbf{\Pi}_A^{\perp}\mathbf{J}$, where

$$\mathbf{J} = \begin{bmatrix} \mathbf{I}_{(L-K)\times(L-K)} \\ \mathbf{0}_{K\times(L-K)} \end{bmatrix}. \tag{13}$$

Put

$$\mathbf{M}_0 = \sigma^{-2}\{\mathbf{\Omega_s}\mathbf{A}^H(\boldsymbol{\theta}_0,\boldsymbol{\rho}_0)\mathbf{R}^{-1}\mathbf{A}(\boldsymbol{\theta}_0,\boldsymbol{\rho}_0)\mathbf{\Omega_s}\}^T \tag{14}$$

so that $\mathbf{M}$ of (9) may be written as $\mathbf{M} = \mathbf{M}_0 \otimes \overline{\mathbf{\Pi}}_A^{\perp}$. Then

$$\begin{aligned}
\mathbf{C}_{\boldsymbol{\theta\theta}} &= \mathrm{Re}\{\mathbf{D}_{\boldsymbol{\theta}}^H\mathbf{M}\mathbf{D}_{\boldsymbol{\theta}}\} = \mathrm{Re}\{\mathbf{D}_{\boldsymbol{\theta}}^H(\mathbf{M}_0\otimes\mathbf{\Pi}_A^{\perp})\mathbf{D}_{\boldsymbol{\theta}}\} \\
&= \mathrm{Re}\{\mathbf{D}_{\boldsymbol{\theta}}^H[\mathbf{M}_0\otimes(\mathbf{B}(\mathbf{B}^H\mathbf{B})^{-1}\mathbf{B}^H)]\mathbf{D}_{\boldsymbol{\theta}}\} \\
&= \mathrm{Re}\{\mathbf{D}_{\boldsymbol{\theta}}^H(\mathbf{I}\otimes\mathbf{B})\,[\mathbf{M}_0\otimes(\mathbf{B}^H\mathbf{B})^{-1}](\mathbf{I}\otimes\mathbf{B})^H\mathbf{D}_{\boldsymbol{\theta}}\} \\
&= [\mathrm{Re}\{\mathbf{D}_{\boldsymbol{\theta}}^H(\mathbf{I}\otimes\mathbf{B})\}, \mathrm{Im}\{\mathbf{D}_{\boldsymbol{\theta}}^H(\mathbf{I}\otimes\mathbf{B})\}] \\
&\quad\times\begin{bmatrix} \mathrm{Re}\{\mathbf{M}_0\otimes(\mathbf{B}^H\mathbf{B})^{-1}\} & -\mathrm{Im}\{\mathbf{M}_0\otimes(\mathbf{B}^H\mathbf{B})^{-1}\} \\ \mathrm{Im}\{\mathbf{M}_0\otimes(\mathbf{B}^H\mathbf{B})^{-1}\} & \mathrm{Re}\{\mathbf{M}_0\otimes(\mathbf{B}^H\mathbf{B})^{-1}\} \end{bmatrix} \\
&\quad\times\begin{bmatrix} \mathrm{Re}\{\mathbf{D}_{\boldsymbol{\theta}}^H(\mathbf{I}\otimes\mathbf{B})\}^T \\ \mathrm{Im}\{\mathbf{D}_{\boldsymbol{\theta}}^H(\mathbf{I}\otimes\mathbf{B})\}^T \end{bmatrix} \\
&= \mathbf{W}\mathbf{M}_c\mathbf{W}^T
\end{aligned} \tag{15}$$

where $\mathbf{I}$ denotes the identity matrix of size $K\times K$, and

$$\mathbf{W} = [\mathrm{Re}\{\mathbf{D}_{\boldsymbol{\theta}}^H(\mathbf{I}\otimes\mathbf{B})\}, \mathrm{Im}\{\mathbf{D}_{\boldsymbol{\theta}}^H(\mathbf{I}\otimes\mathbf{B})\}] \tag{16}$$

$$\mathbf{M}_c = \begin{bmatrix} \mathrm{Re}\{\mathbf{M}_0\otimes(\mathbf{B}^H\mathbf{B})^{-1}\} & -\mathrm{Im}\{\mathbf{M}_0\otimes(\mathbf{B}^H\mathbf{B})^{-1}\} \\ \mathrm{Im}\{\mathbf{M}_0\otimes(\mathbf{B}^H\mathbf{B})^{-1}\} & \mathrm{Re}\{\mathbf{M}_0\otimes(\mathbf{B}^H\mathbf{B})^{-1}\} \end{bmatrix}. \tag{17}$$

Similarly, it can be shown that

$$\mathbf{C}_{\boldsymbol{\rho\theta}} = \mathbf{S}\mathbf{M}_c\mathbf{W}^T \tag{18}$$

$$\mathbf{C}_{\boldsymbol{\rho\rho}} = \mathbf{S}\mathbf{M}_c\mathbf{S}^T \tag{19}$$

where

$$\mathbf{S} = [\mathrm{Re}\{\mathbf{D}_{\boldsymbol{\rho}}^H(\mathbf{I}\otimes\mathbf{B})\}, \mathrm{Im}\{\mathbf{D}_{\boldsymbol{\rho}}^H(\mathbf{I}\otimes\mathbf{B})\}]. \tag{20}$$

Inserting (15), (18), and (19) in (3) and applying the matrix inversion lemma $(\mathbf{A}+\mathbf{BC})^{-1} = \mathbf{A}^{-1} - \mathbf{A}^{-1}\mathbf{B}(\mathbf{I}+\mathbf{CA}^{-1}\mathbf{B})^{-1}\mathbf{CA}^{-1}$, which holds for any size-compatible matrices $\mathbf{A}$, $\mathbf{B}$, and $\mathbf{C}$, and providing all relevant inverses exist

$$\begin{aligned}
&\left[\mathrm{CRB}_{\boldsymbol{\theta}}\right]^{-1} \\
&= N\,[\mathbf{W}\mathbf{M}_c\mathbf{W}^T - \mathbf{W}\mathbf{M}_c\mathbf{S}^T(\mathbf{S}\mathbf{M}_c\mathbf{S}^T + (2N\mathbf{\Omega_\rho})^{-1})^{-1}\mathbf{S}\mathbf{M}_c\mathbf{W}^T] \\
&= N\,\mathbf{W}[\mathbf{M}_c - \mathbf{M}_c\mathbf{S}^T((2N\mathbf{\Omega_\rho})^{-1} + \mathbf{S}\mathbf{M}_c\mathbf{S}^T)^{-1}\mathbf{S}\mathbf{M}_c]\mathbf{W}^T \\
&= N\,\mathbf{W}(\mathbf{M}_c^{-1} + 2N\mathbf{S}^T\mathbf{\Omega_\rho}\mathbf{S})^{-1}\mathbf{W}^T \\
&= \frac{1}{2}\,\mathbf{W}\left(\mathbf{S}^T\mathbf{\Omega_\rho}\mathbf{S} + \frac{1}{2N}\,\mathbf{M}_c^{-1}\right)^{-1}\mathbf{W}^T.
\end{aligned} \tag{21}$$

Note that $\mathbf{M}_c$ of (17) is regular, provided that $\mathbf{M}_0$ in (14) is regular because $\mathbf{M}_0\otimes(\mathbf{B}^H\mathbf{B})^{-1}$ would then be regular as well. Thus, the new CRB expression in (21) is numerically stable for large N, unlike (3).

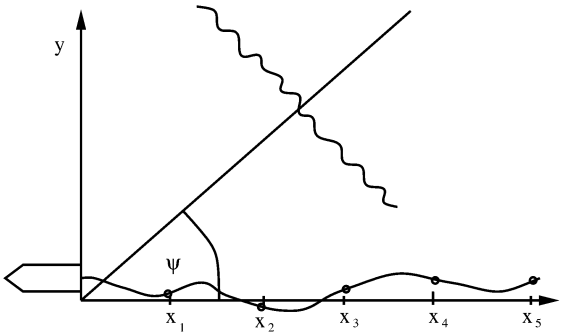

Fig. 1. Coordinate system for a towed-array of hydrophones with one far-field incident source.

The limit-CRB for N going to infinity easily follows:

$$\mathrm{CRB}_{\boldsymbol{\theta}}^{N\to\infty} \overset{\mathrm{def}}{=} \lim_{N\to\infty}\mathrm{CRB}_{\boldsymbol{\theta}} = 2\,[\mathbf{W}(\mathbf{S}^T\mathbf{\Omega_\rho}\mathbf{S})^{-1}\mathbf{W}^T]^{-1}. \tag{22}$$

The limit has the interpretation that it describes the best achievable residual variance of the DOA-estimate due to array uncertainties.

To detail the impact of array-shape uncertainties and of the gain-phase uncertainties on direction-finding accuracy, the subsequent analysis assumes a single incident source (i.e., $K=1$) for mathematical simplicity. Without loss of generality, the nominally linear towed array is assumed to align along the x-axis; hence, the x-axis Cartesian direction-cosine needs be estimated. That is, $\theta = u = \cos\psi$; see Fig. 1. From (2), $\mathbf{a}(\boldsymbol{\theta},\boldsymbol{\rho}) = \mathbf{g}\odot e^{j\boldsymbol{\phi}}$, where $\odot$ denotes the element-wise product, and $\boldsymbol{\phi} = \boldsymbol{\varphi} + 2\pi/\lambda\,(\mathbf{x}\,u + \mathbf{y}\,v + \mathbf{z}\,w)$.

Further assume that uncertainties in the hydrophones' gains, phases, and locations are mutually independent. Then, random deviations of $\boldsymbol{\rho}$ around its nominal value $\boldsymbol{\rho}_0$ have the *a priori* covariance matrix

$$\mathbf{\Omega_\rho} = \mathrm{diag}(\mathbf{\Omega}_{\Delta\mathbf{g}}, \mathbf{\Omega}_{\Delta\varphi}, \mathbf{\Omega}_{\Delta\mathbf{x}}, \mathbf{\Omega}_{\Delta\mathbf{y}}, \mathbf{\Omega}_{\Delta\mathbf{z}}). \tag{23}$$

For the above-defined $\mathbf{a}(\boldsymbol{\theta},\boldsymbol{\rho})$

$$\mathbf{D}_{\boldsymbol{\theta}} = \frac{\partial\mathbf{a}(\boldsymbol{\theta},\boldsymbol{\rho})}{\partial u} = j\,\frac{2\pi}{\lambda}(\mathbf{x}\odot\mathbf{a}(\boldsymbol{\theta}_0,\boldsymbol{\rho}_0)) \tag{24}$$

where $\odot$ denotes the element-wise product, and

$$\begin{aligned}
\mathbf{D}_{\boldsymbol{\rho}} &= \frac{\partial\mathbf{a}(\boldsymbol{\theta},\boldsymbol{\rho})}{\partial\boldsymbol{\rho}} \\
&= \left[\frac{\partial\mathbf{a}(\boldsymbol{\theta},\boldsymbol{\rho})}{\partial\mathbf{g}}, \frac{\partial\mathbf{a}(\boldsymbol{\theta},\boldsymbol{\rho})}{\partial\boldsymbol{\varphi}}, \frac{\partial\mathbf{a}(\boldsymbol{\theta},\boldsymbol{\rho})}{\partial\mathbf{x}}, \frac{\partial\mathbf{a}(\boldsymbol{\theta},\boldsymbol{\rho})}{\partial\mathbf{y}}, \frac{\partial\mathbf{a}(\boldsymbol{\theta},\boldsymbol{\rho})}{\partial\mathbf{z}}\right] \\
&= [\mathrm{diag}(e^{j\boldsymbol{\phi}}), j\mathbf{m}\otimes\mathrm{diag}(\mathbf{a})]
\end{aligned} \tag{25}$$

where

$$\mathbf{m} = \left[1,\ \frac{2\pi}{\lambda}\,u,\ \frac{2\pi}{\lambda}\,v,\ \frac{2\pi}{\lambda}\,w\right]. \tag{26}$$

Note that $\mathbf{M}_0$ of (14) becomes the scalar M_0

$$\begin{aligned}
M_0 &= \sigma^{-2}(\mathbf{\Omega_s}\mathbf{A}^H\mathbf{R}^{-1}\mathbf{A}\mathbf{\Omega_s}) \\
&= \frac{\Omega_s^2}{\sigma^2}\,\mathbf{a}^H(\sigma^2\mathbf{I} + \Omega_s\mathbf{a}\mathbf{a}^H)^{-1}\mathbf{a} \\
&= \frac{\Omega_s^2}{\sigma^2}\,\mathbf{a}^H\left[\frac{1}{\sigma^2}\mathbf{I} - \frac{\Omega_s}{\sigma^4}(1+\sigma^{-2}\Omega_s\|\mathbf{a}\|^2)^{-1}\mathbf{a}\mathbf{a}^H\right]\mathbf{a} \\
&= \frac{\Omega_s^2\|\mathbf{g}\|^2}{\sigma^2(\sigma^2+\Omega_s\|\mathbf{g}\|^2)}.
\end{aligned} \tag{27}$$

In (27), the matrix inversion lemma is used along with $\|\mathbf{a}\| = \|\mathbf{g}\|$. The matrix $\mathbf{B}$, containing the basis of the column-space of $\mathbf{\Pi}_A^{\perp}$, may be chosen arbitrarily. However

$$\mathbf{B} = \mathbf{\Pi}_A^{\perp} \operatorname{diag}(e^{j\boldsymbol{\phi}})\,\mathbf{J} \tag{28}$$

would be a convenient choice,[4] giving

$$\begin{aligned}\mathbf{D}_{\rho}^{H}\mathbf{B} &= \begin{bmatrix} \operatorname{diag}(e^{-j\boldsymbol{\phi}}) \\ -j\mathbf{m}^T \otimes \operatorname{diag}(\mathbf{a}^*) \end{bmatrix} \left[\mathbf{I} - \frac{\mathbf{a}\mathbf{a}^H}{\|\mathbf{a}\|^2}\right] \operatorname{diag}(e^{j\boldsymbol{\phi}})\,\mathbf{J} \\ &= \begin{bmatrix} \mathbf{\Pi}_g^{\perp}\,\mathbf{J} \\ -j\mathbf{m}^T \otimes (\operatorname{diag}(\mathbf{g})\mathbf{\Pi}_g^{\perp}\,\mathbf{J}) \end{bmatrix} = \begin{bmatrix} \mathbf{\Pi}_g^{\perp}\,\mathbf{J} \\ -j\mathbf{m}^T \otimes \mathbf{H} \end{bmatrix} \end{aligned} \tag{29}$$

where

$$\mathbf{\Pi}_g^{\perp} = \mathbf{I} - \frac{\mathbf{g}\mathbf{g}^H}{\|\mathbf{g}\|^2} \tag{30}$$

$$\mathbf{H} = \operatorname{diag}(\mathbf{g})\mathbf{\Pi}_g^{\perp}\,\mathbf{J}. \tag{31}$$

After some algebra, (20), (17), and (16) can be rewritten as

$$\mathbf{S} = \begin{bmatrix} \mathbf{\Pi}_g^{\perp}\,\mathbf{J} & \mathbf{0} \\ \mathbf{0} & -\mathbf{m}^T \otimes \mathbf{H} \end{bmatrix} \tag{32}$$

$$\mathbf{W} = \left[0, -\frac{2\pi}{\lambda}\,\mathbf{x}^T\mathbf{H}\right] \tag{33}$$

$$\mathbf{M}_c = M_0 \begin{bmatrix} (\mathbf{J}\mathbf{\Pi}_g^{\perp}\,\mathbf{J})^{-1} & \mathbf{0} \\ \mathbf{0} & (\mathbf{J}\mathbf{\Pi}_g^{\perp}\,\mathbf{J})^{-1} \end{bmatrix}. \tag{34}$$

Combining (32) and (23)

$$\mathbf{S}^T\mathbf{\Omega}_{\rho}\mathbf{S} = \begin{bmatrix} * & * \\ * & \mathbf{H}^T\mathbf{\Omega}_{\Delta\phi}\mathbf{H} \end{bmatrix} \tag{35}$$

where the blocks denoted by the asterisks are not displayed, and

$$\mathbf{\Omega}_{\Delta\phi} = \mathbf{\Omega}_{\Delta\varphi} + \left(\frac{2\pi}{\lambda}\right)^2 [u^2\,\mathbf{\Omega}_{\Delta x} + v^2\,\mathbf{\Omega}_{\Delta y} + w^2\,\mathbf{\Omega}_{\Delta z}]. \tag{36}$$

Inserting (32)–(35) in (21) gives

$$\begin{aligned}\left[\mathrm{CRB}_{\boldsymbol{\theta}}\right]^{-1} &= \frac{1}{2}\,\mathbf{W}\left(\mathbf{S}^T\mathbf{\Omega}_{\boldsymbol{\rho}}\mathbf{S} + \frac{1}{2N}\,\mathbf{M}_c^{-1}\right)^{-1}\mathbf{W}^T \\ &= \frac{2\pi^2}{\lambda^2}\,\mathbf{x}^T\mathbf{H}\left(\mathbf{H}^T\mathbf{\Omega}_{\Delta\phi}\mathbf{H} + \frac{M_0}{2N}\,\mathbf{J}\mathbf{\Pi}_g^{\perp}\,\mathbf{J}\right)^{-1}\mathbf{H}^T\mathbf{x}. \end{aligned} \tag{37}$$

The CRB depends on the hydrophones' gains by means of the matrix $\mathbf{H}$ defined in (31). It is independent of the uncertainties in the hydrophones' gain $\mathbf{\Omega}_{\Delta g}$ but depends only on $\mathbf{\Omega}_{\Delta\phi}$, which combines the hydrophones' phase uncertainties and location uncertainties. This is because all arrival-angle information is contained in the phase of the data; cf. (2). For multiple sources (i.e, $K > 1$), these uncertainties have more complex interactions; and the general formula in (21) would be necessary.

$N \to \infty$ gives the asymptotic CRB

$$\mathrm{CRB}_{\boldsymbol{\theta}}^{N\to\infty} = \frac{\lambda^2}{2\pi^2}\,[\mathbf{x}^T\mathbf{H}(\mathbf{H}^T\mathbf{\Omega}_{\Delta\phi}\mathbf{H})^{-1}\mathbf{H}^T\mathbf{x}]^{-1}. \tag{38}$$

[4]The exponential term in (28) is allowed because the scaling of the columns of $\mathbf{B}$ is arbitrary due to the projection in (12)

As expected, the limit-CRB is independent of the additive noise's variance σ^2, which drops out along with M_0 of (27). The CRB does depend on the array geometry not only through the vector of sensor coordinates $\mathbf{x}$ but through the error covariance matrix $\mathbf{\Omega}_{\Delta\phi}$ as well, which incorporates the sensor location uncertainties.

IV. New Fluid-Mechanics-Based Statistical Models of a Nominally Linear Towed Array's Shape Deformation

The derivation of the Paidoussis equation in [21] is herein revisited in order to incorporate a new term for the fluid flow's transverse speed and normal speed caused by oceanic streams and swells. The fluid flow's instantaneous normal speed is modeled as an homogenous stationary Gaussian random field with known space-time correlation structure, which may be measured offline and tabulated for different field conditions. This Gaussian assumption is for mathematical simplicity and is not unreasonable because statistical distributions with longer "tails" (thereby implying a higher probability for very high fluid-flow speeds) can hardly be observed here due to fluid viscosity.

The towing vessel transversal motion represents another cause of array deformation. Already accounted for in the original Paidoussis equation, the towing vessel's transversal motion is herein assumed to be due to the vessel's small random maneuvers and is modeled as a Gaussian random field with known space-time correlation structure (which may be measured and tabulated off-line) and as stochastically independent of the fluid flows along the array.

The Paidoussis equation is discretized both in time and in space and consequently used to derive physically meaningful covariance matrices of the sensor location uncertainties, $\mathbf{\Omega}_{\Delta x}$, $\mathbf{\Omega}_{\Delta y}$, and $\mathbf{\Omega}_{\Delta z}$ for use in the quasi-Bayesian CRB. The following developments will consider only small array-shape deformations. Since the tow-cable is assumed neutrally buoyant, the horizontal deformation and the vertical deformation obeys the same differential equation (but possibly with different constants for the two directions). Hence, with no loss in generality, the subsequent analysis will express only the horizontal deformation's $\mathbf{\Omega}_{\Delta y}$ in terms of physically measurable constants. Subsequent simulation examples will assume that $\mathbf{\Omega}_{\Delta z} = \mathbf{\Omega}_{\Delta y}$. Finally, relative longitudinal contractions of the array can be neglected thanks to the small array-shape deformation assumption. It follows that $\mathbf{\Omega}_{\Delta x} \approx \mathbf{0}$.

A. Generic Model of Towed Array Fluid Mechanics

Two causes exist for towed-array deformation: 1) the towing-vessel's transverse motion or varying speed and 2) oceanic swells and currents. The Paidoussis equation [1]–[3], [7], [8], [11], [12] describes the fluid mechanics through which the two above-mentioned factors affect the shape of a towed array. More precisely, the Paidoussis equation describes the dynamical behavior of a flexible and cross-sectionally thin cable towed through a certain fluid:

$$\begin{aligned} m\frac{\partial^2 y(t,x)}{\partial t^2} - \frac{\partial}{\partial x}\left(T(x)\frac{\partial y(t,x)}{\partial x}\right) + f_A(t,x) + f_A(t,x) \\ + f_N(t,x) - f_T(t,x)\,\frac{\partial y(t,x)}{\partial x} + B\frac{\partial^4 y(t,x)}{\partial x^4} = 0. \end{aligned} \tag{39}$$

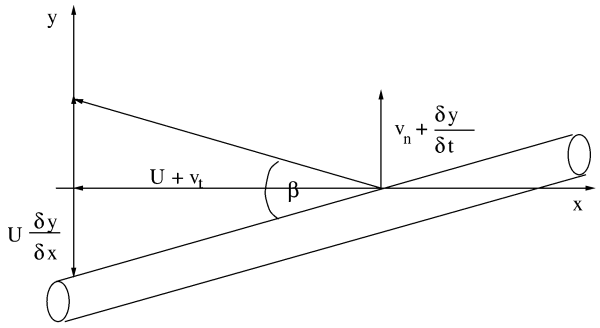

Fig. 2. Enlarged segment of the deformed towed array.

The notation is as follows:

$y(t,x)$	towed-array's transverse displacement at time t and location x along the array's length;
m	towed-array's per-unit-length mass;
$T(x)$	tow-cable's spatially variable tension;
$f_A(t,x)$	inviscid force due to the acceleration of the tow-cable's virtual mass;
$f_N(t,x)$	per-unit-length viscous force acting on the tow-cable in the normal direction;
$f_T(t,x)$	similar force acting in the tangential direction;
B	tow-cable's bending stiffness.

From [11] and [38],

$$f_A(t,x) = M\left[\frac{\partial}{\partial t} + U\,\frac{\partial}{\partial x}\right]^2 y(t,x) \tag{40}$$

$$f_N(t,x) = \frac{M[V(t,x)]^2}{D}\,C_n\,\sin\beta(t,x) \tag{41}$$

$$f_T(t,x) = \frac{M[V(t,x)]^2}{D}\,C_t\cos\beta(t,x) \tag{42}$$

$$\begin{aligned} T(x) &= T(L) - \int_x^L f_T(t,x)dx \\ &= C_t' MU^2 + \int_x^L f_T(t,x)dx \end{aligned} \tag{43}$$

with these notations:

M	displaced fluid's per-unit-length mass;
D	towed-array's cross-sectional diameter;
C_n	towed-array's normal drag coefficient;
C_t	towed-array's tangential drag coefficient;
C_t'	form drag at the trailing end ($=0$ for a free end);
U	tow-vessel's speed along the positive x-axis;
$V(t,x)$	tow-cable's speed relative to distant fluid;
$\beta(t,x)$	angle between the relative velocity of the surrounding fluid flow and the local tangent of the cable.

$\beta(t,x)$ depends on U but also on the fluid flow's transverse speed $v_t(t,x)$ and normal speed $v_n(t,x)$ due to the ocean streams and swells (see Fig. 2).

To summarize, the inputs to the fourth-order partial differential equation in (39) are U, $v_t(t,x)$, and $v_n(t,x)$, under the TPI-motion defined boundary condition $y(t,0)$, and the output is $y(t,x)$: the towed-array's space-time deformed geometry.

Prior researchers (to the best of the authors' knowledge) have overlooked the statistical influence of oceanic currents on array shape deformation in the Paidoussis equation. One contribution of the present work is to rigorously characterize the statistical effects of $v_t(t,x)$ and $v_n(t,x)$ in the Paidoussis equation on the hydrophones' dislocation.

Under the reasonable assumption that the tow-speed greatly exceeds the surrounding water's flow velocity (i.e., $U \gg v_t(t,x)$, $U \gg v_n(t,x)$), it holds that $V(t,x) \approx U$ and $\beta(t,x) \approx 0$. The latter approximation means that hydrophone dislocation is substantial only perpendicular to, but not along, the array axis. Referring to Fig. 2

$$\begin{aligned} \sin\beta(t,x) &\approx \beta(t,x) \\ &\approx \frac{1}{U}\left[\frac{\partial y(t,x)}{\partial t} + U\,\frac{\partial y(t,x)}{\partial x} - v_n(t,x-tU)\right] \end{aligned} \tag{44}$$

$$\cos\beta(t,x) \approx 1 \tag{45}$$

$$T(x) \approx \left(C_t\,\frac{L-x}{D} + C_t'\right) MU^2. \tag{46}$$

Assuming that the tow-cable is sufficiently flexible to neglect the bending stiffness term $B(\partial^4 y(t,x)/\partial x^4)$ in (39), the fourth-order Paidoussis equation in (39) may be reduced to second-order:

$$\begin{aligned} & m\frac{\partial^2 y(t,x)}{\partial t^2} + M\left[\frac{\partial}{\partial t} + U\,\frac{\partial}{\partial x}\right]^2 y(t,x) \\ & - \frac{\partial}{\partial x}\left[\left(C_t\,\frac{L-x}{D} + C_t'\right) MU^2 \frac{\partial y(t,x)}{\partial x}\right] \\ & - \frac{MU^2}{D}\,C_t\,\frac{\partial y(t,x)}{\partial x} \\ & + C_n\frac{MU}{D}\left[\frac{\partial y(t,x)}{\partial t} + U\frac{\partial y(t,x)}{\partial x} - v_n(t,x-tU)\right] = 0. \end{aligned} \tag{47}$$

Moreover, because $D \ll L$, the subsequent analysis will ignore those terms in the above equations that are not inversely proportional to D. This second approximation results in the *small-diameter Paidoussis equation*[5] [21]:

$$\begin{aligned} (x-L)\,\frac{\partial^2 y(t,x)}{\partial x^2} + \frac{C_n}{C_t U}\,\Bigg[&\frac{\partial y(t,x)}{\partial t} \\ &+ U\,\frac{\partial y(t,x)}{\partial x} - v_n(t,x-tU)\Bigg] = 0. \end{aligned} \tag{48}$$

The subsequent analysis will model $v_n(t,x)$ as a two-dimensional random field of Gaussian distribution, with zero mean and an *a priori* known spatio-temporal covariance function. This random field is modeled as statistically stationary over space (i.e., array length) and time; hence, $\mathrm{E}[v_n(t,x)v_n(t',x')] = c_v(t-t', x-x')$, the mathematical form of which reflects oceanic conditions and may be empirically determined. Moreover, this random field may be statistically correlated over time; an illustrative case of AR(1) will be analyzed in detail.

B. Discretizing the Small-Diameter Paidoussis Equation

Toward solving the above partial differential equation, the space-time discretization in [21] and [38] is herein adopted to represent array shape deformation as a finite-dimensional state-

[5]The small-diameter Paidoussis equation in [21] does not include the $-v_n(t, x - tU)$ term in (48) because [21] neglects the effects of oceanic currents.

space, with the towed-point induced temporal motion and the oceanic currents' space-time behavior as the system's driving inputs. Referring to Appendix A for details

$$\underbrace{\begin{bmatrix} y((i+1)H_t,0) \\ y((i+1)H_t,H_x) \\ \vdots \\ y((i+1)H_t,(M_L-1)H_x) \end{bmatrix}}_{=\mathbf{y}(i+1)} = \mathbf{F} \underbrace{\begin{bmatrix} y(iH_t,0) \\ y(iH_t,H_x) \\ \vdots \\ y(iH_t,(M_L-1)H_x) \end{bmatrix}}_{\stackrel{\text{def}}{=}\mathbf{y}(i)} + \underbrace{\begin{bmatrix} u_0(iH_t) \\ 0 \\ \vdots \\ 0 \end{bmatrix}}_{\stackrel{\text{def}}{=}\mathbf{u}(i)} + H_t \underbrace{\begin{bmatrix} v_n(iH_t,-iH_x) \\ v_n(iH_t,-(i-1)H_x) \\ \vdots \\ v_n(iH_t,-(i-M_L+1)H_x) \end{bmatrix}}_{\stackrel{\text{def}}{=}\mathbf{v}(i)} \quad (49)$$

where $\mathbf{F}$ represents the transition matrix, i denotes the discrete-time index, M_L symbolizes the number of discretization steps along the array's length, and $H_x = L/(M_L - 1)$ and $H_t = H_x/U$, respectively, represent the discretization step sizes in space and time. The stochastic vector $\mathbf{u}(i)$ stands for tow-point induced (TPI) motion, where $\{u_0(iH_t)\}_{i=0}^{\infty}$ is a statistically stationary random sequence. Although [21] and [38] model $\{u_0(iH_t)\}_{i=0}^{\infty}$ as a temporally *un*correlated noise sequence, this present work will model $\{u_0(iH_t)\}_{i=0}^{\infty}$ in the mathematically more general and physically more realistic form of a temporally *correlated* random sequence. The stochastic vector $\mathbf{v}(i)$, which is not included in [21] and [38][6] but is newly introduced in this present work, represents the sea water's spatio-temporally correlated currents.

This above discretization scheme serves only as a mathematical technique to solve the partial differential equation in (47) but imposes no presumption on the physical behavior of the towed array. This discretization is to be distinguished from the piecewise linear model of array deformation [22], [23], [29], [33], [34], [40]. The latter array model assumes the towed array to behave like a concatenation of rigid linear segments, jointed at arbitrary angles. The above discretization makes no piecewise assumption regarding array deformation.

Although the transition matrix $\mathbf{F}$ is strictly speaking a tridiagonal matrix (see Appendix A), empirical researchers [21], [24], [36] find it useful to use the first-order approximation

$$\mathbf{F} = \alpha(H_x)\mathbf{L} \quad (50)$$

where $\alpha(H_x)$ (with $0 \le \alpha(H_x) \le 1$) denotes the damping over a length H_x for TPI motion propagating down the array's length, and

$$\mathbf{L} = \begin{bmatrix} 0 & 0 & \cdot & \cdot & 0 \\ 1 & 0 & \cdot & \cdot & \cdot \\ 0 & 1 & 0 & \cdot & \cdot \\ \cdot & \cdot & \cdot & \cdot & \cdot \\ 0 & \cdot & \cdot & 1 & 0 \end{bmatrix}. \quad (51)$$

With respect to the formulation of (50) and (51) developed in [21], [36], and [38], the present paper offers the following new insight: The length-dependent damping coefficient α is physically related to H_x such that $\alpha(H_x + H_x') = \alpha(H_x)\alpha(H_x')$ for any arbitrary positive numbers H_x and H_x'; hence, $\alpha(H_x)$ must take on the mathematical form of an exponential function of H_x, i.e.,

$$\alpha(H_x) = e^{-C_\alpha H_x} \quad (52)$$

when C_α represents an empirically measurable constant dependent only on the sea water's and the array's physical properties, namely, on C_t and C_n. A smaller C_α means less damping of towed-point induced or ocean-induced transverse motion along the array's length. For notational simplicity, the argument H_x will be omitted from α wherever possible.

C. Solving for the Towed-Array's Space-Time Shape Deformation

This subsection advances an original solution to (49) for $\mathbf{u}(i)$ and $\mathbf{v}(i)$ that is stationary and stochastically independent. Note that the tow-point's transverse displacement has been empirically determined to propagate down the array at close to the tow-boat's speed with little damping [21], [36]. Equation (49) has a bounded (in the least square sense) solution $\mathbf{y}(i)$, provided that $\|\mathbf{F}\| < 1$ for some matrix norm $\|\cdot\|$. Hence

$$\mathbf{y}(i) = \underbrace{\sum_{j=0}^{\infty} \mathbf{F}^j \mathbf{u}(i-j)}_{\stackrel{\text{def}}{=}\mathbf{u}_F(i)} + \underbrace{\sum_{j=0}^{\infty} \mathbf{F}^j \mathbf{v}(i-j)}_{\stackrel{\text{def}}{=}\mathbf{v}_F(i)}. \quad (53)$$

For the $\mathbf{F}$ in (50), the condition $\|\mathbf{F}\| < 1$ is equivalent to $\alpha < 1$.

From the independence assumption for $\mathbf{u}(i)$ and $\mathbf{v}(i)$, the hydrophones' location uncertainties have the following spatio-temporal covariance

$$\underbrace{\text{cov}[\mathbf{y}(i)]}_{\stackrel{\text{def}}{=}\mathbf{C}_\mathbf{y}} = \underbrace{\text{cov}[\mathbf{u}_F(i)]}_{\stackrel{\text{def}}{=}\mathbf{C}_{\mathbf{u}_F}} + \underbrace{\text{cov}[\mathbf{v}_F(i)]}_{=\text{def}\mathbf{C}_{\mathbf{v}_F}}. \quad (54)$$

The hydrophones' dislocation covariances may thus be determined once the specific form of the above two right-hand-side terms are known, perhaps from empirical measurements or databases. The above entities are not functions of i because of the temporal stationarity assumption.

The towing-vessel's motion and the oceanic currents represent statistically independent inputs to the towed-array system in (47) and (53); hence, the system's output equals (as expected) a sum of the system outputs due separately to either input. The main problem solved in the section is to express the above terms $\mathbf{C}_{\mathbf{u}_F}$ and $\mathbf{C}_{\mathbf{v}_F}$ in terms of the covariance of the TPI motion $\mathbf{C}_\mathbf{u}$ and covariance matrices of instantaneous fluid speeds $\mathbf{C}_\mathbf{v}$, which are assumed to be known.

For hydrophones nominally at $\{x_1, \ldots, x_L\}$ from the tow-point, where $x_m = \xi_m H_x$ for integers $\{\xi_m, m = 1, \ldots, L\}$, define $[\mathbf{C}_\mathbf{y}]_{\xi_\ell,\xi_m} \stackrel{\text{def}}{=} \text{cov}[y(t,x_\ell), y(t,x_m)]$ for $\ell, m = 1, \ldots, L$. Notice that $[\mathbf{C}_\mathbf{y}]_{\xi_\ell,\xi_m}$ is the (ℓ,m)th element of the desired matrix $\mathbf{\Omega}_{\Delta y}$. Under assumption (54), $[\mathbf{C}_\mathbf{y}]_{\xi_\ell,\xi_m}$ may be expressed as $[\mathbf{C}_{\mathbf{u}_F}]_{\xi_\ell,\xi_m} + [\mathbf{C}_{\mathbf{v}_F}]_{\xi_\ell,\xi_m}$, where the first term is due to TPI motion, and the second term is due to oceanic currents. The

[6]Instead, [21] and [38] have a statistically stationary and spatio-temporally *un*correlated driving input as a "catch-all" function to include all modeling errors.

form of $[\mathbf{C}_{\mathbf{u}_F}]_{\xi_\ell,\xi_m}$ remains to be derived from the spatio-temporal statistics of $\mathbf{u}_F$ as well as $[\mathbf{C}_{\mathbf{v}_F}]_{\xi_\ell,\xi_m}$ from the spatio-temporal statistics of $\mathbf{v}_F$. Each term is to be studied separately below, with detailed attention given to the particular illustrative case of first-order autoregressive auto-covariances for the TPI motion and of oceanic current velocities. The resulting covariances $[\mathbf{C}_{\mathbf{y}}]_{\xi_\ell,\xi_m}$ turn out to be largely independent of the space-time discretization, assuming the discretization to be sufficiently fine.

D. New Statistical Modeling of Tow-Point Induced Towed-Array Shape-Deformation

The towing-vessel's motion has been modeled in [21] as temporally uncorrelated, which may be physically unrealistic for high time-sampling rates. Instead, the analysis here allows arbitrary temporal correlation (but requires statistical stationarity) in the towing-vessel's motion. The following expresses $\mathbf{C}_{\mathbf{u}_F}$ in terms of the spatio-temporal statistics of $\mathbf{u}_F$, first for the general case of any statistically stationary (but otherwise arbitrary) spatio-temporal covariance and then for the special case of a first-order auto-regressive temporal covariance. All subsequent expressions will turn out to be independent of the discretization grid used earlier.

Assume that $\{u_0(iH_t)\}_{i=1}^{\infty}$ is statistically stationary, zero-mean, and with a Toeplitz covariance matrix $\mathbf{C}_u$ containing elements $[\mathbf{C}_u]_{i,j} = \mathrm{E}[u_0(iH_t)u_0(jH_t)]$ for $i,j = 1,\ldots,M_L$. Hence

$$\begin{aligned}\mathbf{u}_F(i) &= \sum_{j=0}^{\infty} \mathbf{F}^j\, \mathbf{u}(i-j) \\ &= \Big[u_0(iH_t),\, \alpha u_0((i-1)H_t)),\ldots,\alpha^{M_L-1}u_0((i-M_L+1)H_t)\Big]^T\end{aligned} \tag{55}$$

and $\mathbf{u}_F(i)$ has the spatial covariance matrix $\mathbf{C}_{\mathbf{u}_F} = \mathbf{F}_\alpha \mathbf{C}_u \mathbf{F}_\alpha$, where $\mathbf{F}_\alpha = \mathrm{diag}[1,\alpha,\alpha^2,\ldots,\alpha^{M_L-1}]$. Thus

$$[\mathbf{C}_{\mathbf{u}_F}]_{\xi_\ell,\xi_m} = \alpha^{\xi_\ell+\xi_m-2}[\mathbf{C}_u]_{\xi_\ell,\xi_m}, \quad \ell,m = 1,\ldots,L. \tag{56}$$

The above equation constitutes this subsection's main contribution, relating the positional uncertainty's covariance function to the TPI motion's spatio-temporal covariance function.

For the special case where the TPI motion may be represented as an AR(1) temporally random process,[7]

$$[\mathbf{C}_u]_{\xi_\ell,\xi_m} = \sigma_u^2\, e^{-C_u|\xi_\ell-\xi_m|H_t}, \quad \ell,m = 1,\ldots,L \tag{57}$$

where C_u and σ_u^2 represent constants that may be empirically measured: σ_u^2 denotes the variance of the TPI motion, and C_u characterizes the time correlation of the TPI motion. Given C_u, the time delay Δt [in which the correlation between $u_0(t)$ and $u_0(t+\Delta t)$ decays to 1/10] equals $\log 10/C_u$. Combining (52), (56), and (57)

$$\begin{aligned}[\mathbf{C}_{\mathbf{u}_F}]_{\xi_\ell,\xi_m} &= [e^{-C_\alpha H_x}]^{(\xi_\ell+\xi_m-2)}\, \sigma_u^2\, e^{-C_u|\xi_\ell-\xi_m|H_t} \\ &= \sigma_u^2 e^{-C_\alpha(x_\ell+x_m)-C_u|x_\ell-x_m|/U} e^{-2C_\alpha H_x} \\ &\to \sigma_u^2 e^{-C_\alpha(x_\ell+x_m)-C_u|x_\ell-x_m|/U},\ H_x \to 0\end{aligned} \tag{58}$$

and may be substituted into (54) to give the towed-array's space-time shape-deformation covariance. The expression on the right-hand side of (58) is the covariance element for an infinitely fine discretization grid.

[7]For covariance functions of the general AR(i) form or the general ARMA(i, j) form, see [37].

E. Statistical Modeling of Ocean-Induced Array Shape Deformation

The following will express $\mathbf{C}_{\mathbf{v}_F}$ in terms of the spatio-temporal statistics of $v_n(t,x)$, first for the general case stipulating only statistical stationarity and then for the special case where the auto-correlation of $v_n(t,x)$ is AR(1) in both space and time.

Define $\mathbf{C}_{\mathbf{v}}(j) \stackrel{\mathrm{def}}{=} \mathrm{E}\{\mathbf{v}(t)\mathbf{v}^T(t+j)\}$, for $j = 0,\pm1,\pm2\ldots$. With the spatio-temporal covariance function $c_v(t,x)$ of the space-time random field $v_n(t,x)$ characterizing fluid flow, (49) implies $[\mathbf{C}_{\mathbf{v}}(j)]_{\ell,m} = H_t^2\, c_v(jH_t,\,(m-\ell-j)H_x)$ for $\ell,m = 1,\ldots,M_L$. Define

$$\tilde{\mathbf{C}}_{\mathbf{v}}(j) = \sum_{m=0}^{\infty} \mathbf{F}^m\, \mathbf{C}_{\mathbf{v}}(j)(\mathbf{F}^m)^T = \sum_{m=0}^{M_L-1} \mathbf{F}^m\, \mathbf{C}_{\mathbf{v}}(j)(\mathbf{F}^m)^T. \tag{59}$$

The last equality holds because $\mathbf{F}^m = 0$ for $m \geq M_L$, given $\mathbf{F}$ defined in (50). As $\mathbf{C}_{\mathbf{v}}(j)$ is Toeplitz, some straightforward manipulation gives

$$[\tilde{\mathbf{C}}_{\mathbf{v}}(j)]_{\ell,m} = [\mathbf{C}_{\mathbf{v}}(j)]_{\ell,m}\, \frac{1-\alpha^{\min\{\ell,m\}}}{1-\alpha},\ \ell,m=1,\ldots,M_L. \tag{60}$$

Referring to (50), (53), and (59)

$$\begin{aligned}\mathbf{C}_{\mathbf{v}_F} &= \sum_{\ell=0}^{\infty}\sum_{m=0}^{\infty} \mathbf{F}^\ell \mathrm{E}[\mathbf{v}(i-\ell)\mathbf{v}^T(i-m)]\,(\mathbf{F}^m))^T \\ &= \sum_{\ell=0}^{\infty}\sum_{m=0}^{\infty} \mathbf{F}^\ell \mathbf{C}_{\mathbf{v}}(\ell-m)\,(\mathbf{F}^m)^T \\ &= \tilde{\mathbf{C}}_{\mathbf{v}}(0) + \sum_{m=1}^{M_L-1} [\mathbf{F}^m \tilde{\mathbf{C}}_{\mathbf{v}}(m) + \tilde{\mathbf{C}}_{\mathbf{v}}(-m)(\mathbf{F}^m)^T].\end{aligned} \tag{61}$$

The above equation represents this subsection's key contribution, relating the positional uncertainty's covariance function to the oceanic flow's space-time covariance function.

Consider the illustrative case of $v_n(t,x)$ being AR(1) in both space and time

$$c_v(t,x) = \sigma_v^2\, e^{-C_{vt}t - C_{vx}x} \tag{62}$$

where σ_v^2, C_{vt}, and C_{vx} are physical constants that may be empirically measured. σ_v^2 is the total variance of oceanic flows, whereas C_{vt} and C_{vx} determine the correlation length of the random field $v_n(t,x)$ in reference to, respectively, time and space; cf. (57).

Referring to Appendix B for details, for $\xi_\ell = x_\ell/H_x$, $\xi_m = x_m/H_x$, $x_\ell < x_m$, and $H_x \to 0$,

$$
\begin{aligned}
&[\mathbf{C}_{\mathbf{v}_F}]_{\xi_\ell,\xi_m} \\
&\approx \frac{\sigma_v^2 e^{-C_{vx}|x_\ell - x_m|}}{C_\alpha U}\left\{\frac{1}{C_{vt}}\Big[e^{-(C_\alpha + C_{vt}/U)x_\ell} + e^{-(C_\alpha + C_{vt}/U)x_m}\right. \\
&\quad \left. - e^{-C_\alpha x_\ell} - e^{-(C_\alpha + C_{vt}/U)(x_m - x_\ell)}\Big)\Big] \right. \\
&\quad + \frac{1}{C_\alpha U + C_{vt}}\Big[2 - e^{-(C_\alpha + C_{vt}/U)x_\ell} - e^{-(C_\alpha + C_{vt}/U)x_m} \\
&\quad \left. - e^{-C_\alpha x_\ell}(1 - e^{-(C_\alpha + C_{vt}/U)(x_m - x_\ell)})\Big]\right\} \qquad (63)
\end{aligned}
$$

and may be substituted into (54) to give the towed-array's space-time shape-deformation covariance.

F. Summary of Notations of Constants

For easy reference, the following summarizes the notations used in the above two subsections to describe the AR(1,1) oceanic-current model and the AR(1) TPI-motion model.

σ_u^2	variance of the TPI motion;
C_u	constant characterizing the temporal correlation of the TPI motion (57);
σ_v^2	variance of the oceanic flows;
C_{vt}	constant characterizing the temporal correlation of the oceanic flows (62);
C_{vx}	constant characterizing the per-unit-length correlation of the TPI motion (62);
H_α	constant in the exponential dumping model (52).

V. Numerical Examples

A. Example 1: Variance of Positional Deviation Along the Towed-Array

Fig. 3 plots $[\mathbf{C}_{\mathbf{u}_F}]_{x,x}$ and $[\mathbf{C}_{\mathbf{v}_F}]_{x,x}$ along the array's length x when the towing-vessel's motion is an AR(1) temporal stochastic process and when the oceanic currents may be modeled as a spatio-temporal AR(1) space-time stochastic process. The simulation parameters are as follows: The towed-array has the damping parameter $C_\alpha = 0.008$ (m^{-1}) (corresponding to a damping factor $\alpha = 0.95$ per 6.25 m of tow-array length [24]), the TPI-motion has the variance $\sigma_u^2 = 1$ (m^2) and $C_u = 1$ (s^{-1}), the ocean-induced motion has variance $\sigma_v^2 = 0.01$ (m^2) and $C_{vx} = 1$ (m^{-1}) and $C_{vt} = 1$ (s^{-1}).

As x increases (i.e., further from the tow point), the TPI motion becomes less significant, but the oceanic flow becomes more important. A faster tow speed does not affect $[\mathbf{C}_\mathbf{y}]_{x,x}$, which is intuitively reasonable as the angle $\beta(t,x)$ between the array and surrounding fluid's relative velocity also decreases with increasing tow-speed, thereby diminishing the influence of the oceanic currents.

The following examples illustrate the dependence of the CRB of u on various physical parameters in the far-field deep-sea single-source scenario, where the towed-array has uniform half-wavelength spaced hydrophones moving along the x-axis.

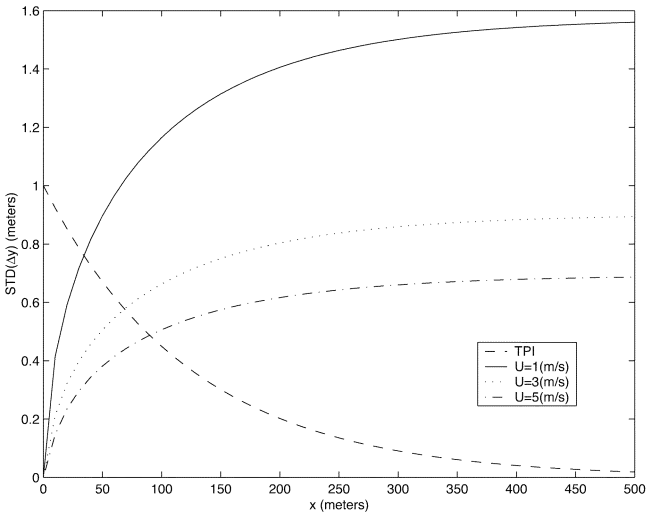

Fig. 3. Standard deviation of positional deviation along the towed-array. Dashed line: Influence from TPI motion. Solid line: Influence from fluid-flows for tow-speeds shown. Referring to (52), (57), and (62), $C_\alpha = 0.008$ $\sigma_u^2 = 1$ (m^2), $C_u = 1$ (m^{-1}), $\sigma_u^2 = 0.01$ (m^{-1}), $C_{vt} = 1$ (s^{-1}), and $C_{vx} = 1$ (m^{-1}). The tow speed is $U = 1$, 3 and 5 (m/s), respectively.

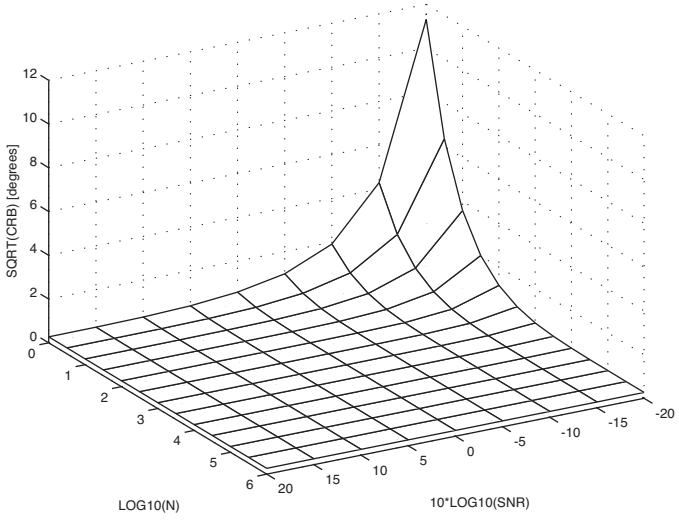

Fig. 4. Square root of CRB (in degrees) versus the number of observation snapshots N and versus the SNR Ω_s/σ_n^2.

B. Example 2: CRB versus the SNR and Number of Snapshots n

Fig. 4 plots the square root of the CRB (in degrees) versus the SNR $= \Omega_s/\sigma_n^2$ and the number of snapshots N. The array has $L = 25$ hydrophones, equispaced at 6.25 m (corresponding to a frequency of 120 Hz [24]) and towed with speed $U = 3$ m/s. The hydrophones' phase uncertainties are uncorrelated with a 3° standard deviation, implying $\mathbf{\Omega}_{\Delta\varphi} = (3\pi/180)^2\mathbf{I}$ (rad^2). All other simulation parameters remain the same as in Example 1. Fig. 4 shows that for SNR > 0 dB, the CRB approximates the large-N limit-CRB, even at $N = 1$. Moreover, the limit-CRB does not depend on the SNR.

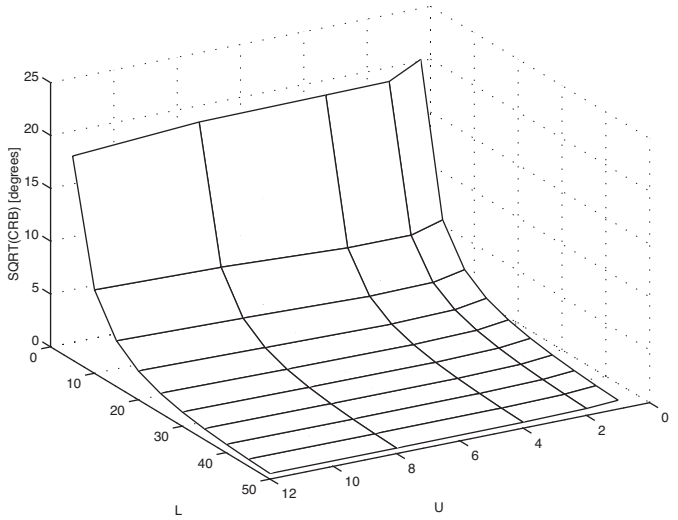

Fig. 5. Square root of the limit-CRB (with $N \to \infty$) versus the number of hydrophones L and versus the tow-speed U.

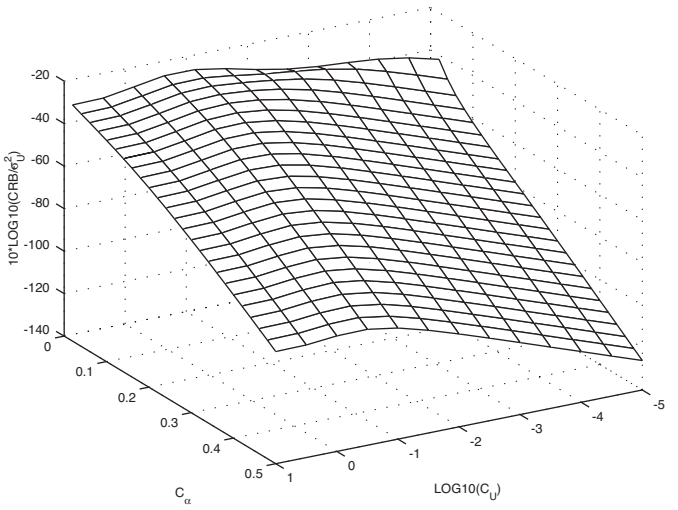

Fig. 6. Limit-CRB (with $N \to \infty$) per unit TPI-motion's variance (in the absence of oceanic currents) versus the TPI-motion parameter C_u and versus the towed-array transversal movement's damping parameter C_α.

C. Example 3: CRB Versus Number of Hydrophones l and Tow-Speed u

Fig. 5 plots the large-N limit-CRB versus the towed-array's number of constituent hydrophones L and the tow-speed U (m/s^{-1}). All other simulation parameters remain identical as in Example 2. As expected, the CRB in Fig. 5 decreases (i.e., the potentially achievable accuracy improves) with more hydrophones and a faster tow-speed.

With at least 30 hydrophones in the towed-array and at low tow-speed, adding more hydrophones to the towed-array (while maintaining the towed-array's half-wavelength inter-hydrophone spacing) will offer more improvement in the direction-finding's CRB when the tow-speed is faster than when the tow-speed is slower.

D. Example 4: CRB versus the TPI Parameters

Fig. 6 plots the large-N limit-CRB versus the TPI-motion parameter C_u (s^{-1}) and the damping parameter C_α (m^{-1}) in the absence of oceanic currents and hydrophone gain/phase uncertainties. The TPI motion is statistically independent but identically distributed along the y- and z-axes. The limit-CRB, which is plotted in Fig. 6, is proportional to the TPI transversal motion's variance σ_u^2 but is independent of the SNR. The CRB also depends significantly on C_α but only slightly on C_u. Recall that $C_u \approx 0$ (m^{-1}) means low-frequency TPI-motions (say, due to the towing vessel's slow maneuvers) and a moderate C_u corresponds to TPI-motions similar to white noise. For fixed C_α, the CRB has a broad plateau with respect to C_u.

E. Example 5: CRB Versus the Oceanic-Current Parameters

Fig. 7 plots the large-N limit-CRB in the absence of TPI motion and hydrophone gain/phase uncertainties versus the oceanic current parameters C_{vx} and C_{vt} for oceanic current that is statistically independent and identically distributed in the vertical and horizontal directions. All other simulation parameters remain the same, as in the previous example. The CRB, which is plotted in Fig. 7, decreases with increasing C_{vx} and with increasing C_{vt}, as expected. For $C_{vx} \approx 0$ (m^{-1}) and $C_{vt} \approx 0$

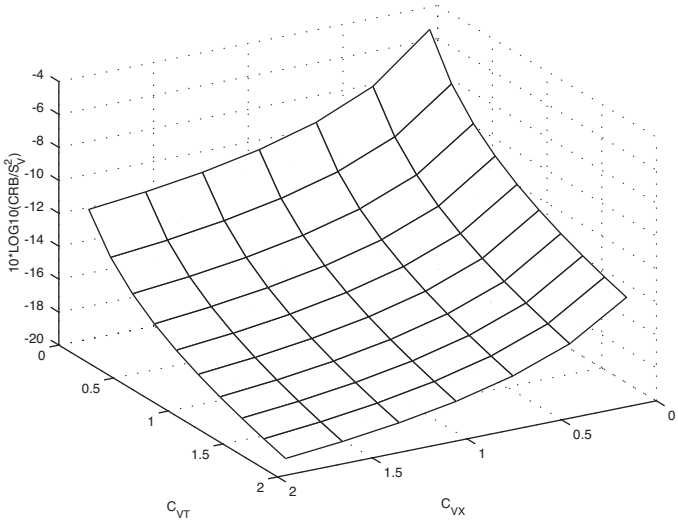

Fig. 7. Limit-CRB (with $N \to \infty$) per unit oceanic current's variance (assuming no TPI motion) plotted versus oceanic motion's AR(1) space-time parameters C_{vt} and C_{vx}.

(s^{-1}), the oceanic current's velocities are more correlated over space and over time, implying that the instantaneous velocities $v_n(t,x)$ and $v_n(t+\Delta t, x+\Delta x)$ are more likely to have the same sign, and array deformation would consequentially have a larger variance.

VI. Conclusion

This work represents an initial step to bridge a serious literature gap in deformed towed-array direction-finding performance analysis by incorporating into the statistical measurement model several essential fluid-mechanics considerations while deriving mathematically rigorous quantitative expressions and qualitative insights into how DOA estimation may depend on physically measurable sources of array deformation. Among various derived properties of the far-field deep-water single-source CRB, especially noteworthy is its independence from the hydrophones' gain uncertainties.

$$
\begin{aligned}
[\mathbf{C}_{\mathbf{v}_F}]_{k\ell} &= [\mathbf{C}_{\mathbf{v}_2}(0)]_{k\ell} + \sum_{m=1}^{M_L-1} [\mathbf{F}^k \mathbf{C}_{\mathbf{v}_2}(m)] + \mathbf{C}_{\mathbf{v}_2}(-m)(\mathbf{F}^m)^T]_{k\ell} \\
&= [\mathbf{C}_{\mathbf{v}_2}(0)]_{k\ell} + \sum_{m=1}^{k-1} \alpha^m [\mathbf{C}_{\mathbf{v}_2}(m)]_{k-m,\ell} + \sum_{m=1}^{\ell-1} \alpha^m [\mathbf{C}_{\mathbf{v}_2}(-k)]_{k,\ell-m} \\
&= H_t^2 \left\{ \mathbf{C}_{\mathbf{v}}(0,(\ell-k)H_x) + \sum_{m=1}^{k-1} \alpha^m \mathbf{C}_{\mathbf{v}}(mH_t,(\ell-k)H_x) \frac{1-\alpha^{k-m}}{1-\alpha} \right. \\
&\quad \left. + \sum_{m=1}^{\ell-1} \alpha^m \mathbf{C}_{\mathbf{v}}(mH_t,(\ell-k)H_x) \frac{1-\alpha^{\min(\ell-m,k)}}{1-\alpha} \right\} \\
&= H_t^2 \left\{ \mathbf{C}_{\mathbf{v}}(0,(\ell-k)H_x) + \sum_{m=1}^{k-1} \alpha^m \mathbf{C}_{\mathbf{v}}(mH_t,(\ell-k)H_x) \frac{1-\alpha^{k-m}}{1-\alpha} \right. \\
&\quad + \sum_{m=1}^{\ell-k} \alpha^m \mathbf{C}_{\mathbf{v}}(mH_t,(\ell-k)H_x) \frac{1-\alpha^{k}}{1-\alpha} \\
&\quad \left. + \sum_{m=\ell-k+1}^{\ell} \alpha^m \mathbf{C}_{\mathbf{v}}(mH_t,(\ell-k)H_x) \frac{1-\alpha^{\ell-m}}{1-\alpha} \right\} \\
&= H_t^2 \sigma_v^2 e^{-C_{vx}(\ell-k)H_x} \left\{ 1 + \sum_{m=1}^{k-1} \alpha^m \frac{1-\alpha^{k-m}}{1-\alpha} e^{-C_{vt}mH_t} \right. \\
&\quad \left. + \sum_{m=1}^{\ell-k} \alpha^m \frac{1-\alpha^{k}}{1-\alpha} e^{-C_{vt}mH_t} + \sum_{m=\ell-k+1}^{\ell} \alpha^m \frac{1-\alpha^{\ell-m}}{1-\alpha} e^{-C_{vt}mH_t} \right\}. \qquad (70)
\end{aligned}
$$

APPENDIX A

Discretization of the Paidoussis equation is achieved [21], [36] by substituting $t = iH_t$ and $x = mH_x$ in the Euler approximation

$$\frac{\partial y(t,x)}{\partial t} \approx \frac{\mathbf{y}_m(i+1) - \mathbf{y}_m(i)}{H_t} \qquad (64)$$

$$\frac{\partial y(t,x)}{\partial x} \approx \frac{\mathbf{y}_m(i) - \mathbf{y}_{m-1}(i)}{H_x} \qquad (65)$$

$$\frac{\partial^2 y(t,x)}{\partial x^2} \approx \frac{\mathbf{y}_m(i) - 2\mathbf{y}_{m-1}(i) + \mathbf{y}_{m-2}(i)}{H_x^2} \qquad (66)$$

where $\mathbf{y}_m(i)$ denotes the $(m+1)$th element of $\mathbf{y}(i)$ in (49). After some manipulations

$$
\begin{aligned}
\mathbf{y}_m(i+1) &= \mathbf{y}_{m-1}(i) + H_t v_n(iH_t, mH_x - iH_t U) \\
&\quad + \frac{C_t}{C_n} \frac{L - mH_x}{H_x} [\mathbf{y}_m(i) - 2\mathbf{y}_{m-1}(i) + \mathbf{y}_{m-2}(i)]. \qquad (67)
\end{aligned}
$$

The last equation may be written in matrix form as (49), where

$$\mathbf{F} = \mathbf{L} + \mathbf{D}_D(\mathbf{I} - 2\mathbf{L} + \mathbf{L}^2) \qquad (68)$$

where $\mathbf{L}$ is defined in (51), and $\mathbf{D}_D = \mathrm{diag}(\delta_1, \delta_2, \ldots, \delta_{M_L})$ is a diagonal matrix with

$$\delta_m = \frac{C_t}{C_n} \frac{L - mH_x}{H_x}, \qquad m = 1, \ldots, M_L. \qquad (69)$$

In [21], [24], and [36] replacing (68) by $\mathbf{F} = \alpha\mathbf{L}$ with a scalar correcting factor α is suggested.

APPENDIX B

Let $x_1 = kH_x$ and $x_k = \ell H_x$, $k \le \ell$. Then, we have (70), shown at the top of the page. Further simplification is obtained by the Taylor series expansion, which is valid for small H_x

$$1 - \alpha = 1 - e^{-C_\alpha H_x} \approx C_\alpha H_x = C_\alpha U H_t$$

and for an arbitrary $|\gamma| < 1$, it holds that

$$\sum_{m=1}^{k-1} \gamma^m = \gamma \frac{1-\gamma^{k-1}}{1-\gamma.}$$

REFERENCES

[1] M. P. Paidoussis, "Dynamics of flexible slender cylinder in axial flow, Part I: Theory," *J. Fluid Mech.*, vol. 26, pp. 717–736, 1966.

[2] ——, "Dynamics of flexible slender cylinder in axial flow, Part II: Experiment," *J. Fluid Mechan.*, vol. 26, pp. 737–751, 1966.

[3] ——, "Dynamics of cylindrical structures subject to axial flow," *J. Sound Vibr.*, vol. 29, pp. 365–385, 1973.

[4] M. J. Hinich, "Bearing estimation using a perturbed linear array," *J. Acoust. Soc. Amer.*, vol. 61, no. 6, pp. 1540–1544, June 1977.

[5] P. M. Schultheiss and J. P. Ianniello, "Optimum range & bearing estimation with randomly perturbed arrays," *J. Acoust. Soc. Amer.*, vol. 68, no. 1, pp. 167–173, July 1980.

[6] N. L. Owsley, "Shape estimation for a flexible underwater cable," in *Proc. IEEE EASCON Conf.*, 1981.

[7] R. M. Kennedy, "Crosstrack dynamics of a long cable towed in the ocean," in *Proc. IEEE Oceans Conf.*, 1981, pp. 966–981.

[8] R. M. Kennedy and E. S. Strahan, "A linear theory of transverse cable dynamics at low frequencies," Naval Underwater Syst. Center, New London, CT, NUSC Tech. Rep. 6463, 1981.

[9] Y. Rockah and P. M. Schultheiss, "Array shape calibration using sources in unknown locations–Part I: Far-field sources," *IEEE Trans. Acoust., Speech, Signal Processing*, vol. ASSP–35, pp. 286–299, Mar. 1987.

[10] ——, "Array shape calibration using sources in unknown locations–Part II: Near-field sources and estimator implementation," *IEEE Trans. Acoust., Speech, Signal Processing*, vol. ASSP-35, pp. 724–735, June 1987.
[11] A. P. Dowling, "The dynamics of towed flexible cylinders, Part I: Neutrally buoyant elements," *J. Fluid Mech.*, vol. 187, pp. 507–532, 1988.
[12] ——, "The dynamics of towed flexible cylinders, Part II: Negatively buoyant elements," *J. Fluid Mech.*, vol. 187, pp. 533–571, 1988.
[13] E. C. van Ballegooijen, G. W. M. van Mierlo, C. van Schooneveld, P. P. M. van der Zalm, A. T. Parsons, and N. H. Field, "Measurement of towed array position, shape and altitude," *IEEE J. Ocean. Eng.*, vol. 14, pp. 375–383, Oct. 1989.
[14] A. J. Weiss and B. Friedlander, "Array shape calibration using sources in unknown locations — A maximum likelihood approach," *IEEE Trans. Signal Processing*, vol. 37, pp. 1958–1966, Dec. 1989.
[15] B. Wahlberg, B. Ottersten, and M. Viberg, "Robust signal parameter estimation in the presence of array perturbations," in *Proc. IEEE Int. Conf. Acoust., Speech, Signal Processing*, 1991, pp. 3277–3280.
[16] B. E. Howard and J. M. Syck, "Calculation of the shape of a towed underwater acoustic array," *IEEE J. Ocean. Eng.*, vol. 17, pp. 193–203, Apr. 1992.
[17] A. L. Swindlehurst and T. Kailath, "A performance analysis of subspace-based methods in the presence of model errors, Part I: The MUSIC algorithm," *IEEE Trans. Signal Processing*, vol. 40, pp. 1758–1773, July 1992.
[18] S. Marcos, "Calibration of a distorted towed array using a propagator operator," *J. Acoust. Soc. Amer.*, pt. 1, vol. 93, no. 4, pp. 1987–1994, Apr. 1993.
[19] S. Li and P. M. Schultheiss, "Depth measurement of remote sources using multipath propagation," *IEEE J. Ocean. Eng.*, vol. 18, pp. 379–387, Oct. 1993.
[20] B. H. Maranda and J. A. Fawcett, "The localization accuracy of a horizontal array observing a narrowband target with partial coherence," *IEEE J. Ocean. Eng.*, vol. 18, pp. 466–473, Oct. 1993.
[21] D. A. Gray, B. D. O. Anderson, and R. R. Bitmead, "Towed array shape estimation using kalman filters — Theoretical models," *IEEE J. Ocean. Eng.*, vol. 18, pp. 543–556, Oct. 1993.
[22] B. G. Quinn, R. F. Barrett, P. J. Kootsookos, and S. J. Searle, "The estimation of the shape of an array using a hidden Markov model," *IEEE J. Ocean. Eng.*, vol. 18, pp. 557–564, Oct. 1993.
[23] B. G. Ferguson, "Remedying the effects of array shape distortion on the spatial filtering of acoustic data from a line array of hydrophones," *IEEE J. Ocean. Eng.*, vol. 18, pp. 565–571, Oct. 1993.
[24] J. L. Riley and D. A. Gray, "Towed array shape estimation using kalman filters—Experimental investigations," *IEEE J. Ocean. Eng.*, vol. 18, pp. 572–581, Oct. 1993.
[25] D. E. Wahl, "Towed array shape estimation using frequency-wavenumber data," *IEEE J. Ocean. Eng.*, vol. 18, pp. 582–590, Oct. 1993.
[26] G. S. Edelson and D. W. Tufts, "Passive localization using a spatially-referenced towed array," in *Proc. IEEE Oceans Conf.*, vol. 2, 1993, pp. 218–223.
[27] N. C. Wyeth, "Methods of array element localization for a towed underwater acoustic array," *IEEE J. Ocean. Eng.*, vol. 19, pp. 128–133, Jan. 1994.
[28] M. Viberg and A. L. Swindlehurst, "Analysis of the combined effects of finite samples and model errors on array processing performance," *IEEE Trans. Signal Processing*, vol. 42, pp. 3073–3083, Nov. 1994.
[29] ——, "A bayesian approach to auto-calibration for parametric array signal processing," *IEEE Trans. Signal Processing*, vol. 42, pp. 3495–3507, Dec. 1994.
[30] S. Narasimhan and J. L. Krolik, "A Cramér-Rao bound for source range estimation in a random ocean waveguide," in *Proc. IEEE Workshop Stat. Signal Array Processing*, 1994, pp. 309–312.
[31] B. Porat, *Digital Processing of Random Signals, Theory & Methods*. Englewood Cliffs, NJ: Prentice-Hall, 1994.
[32] J. Tabrikjan and H. Messer, "Three-dimensional source localization in a waveguide," *IEEE Trans. Signal Processing*, vol. 44, pp. 1–13, Jan. 1996.
[33] J. J. Smith, Y. H. Leung, and A. Cantoni, "The Cramér-Rao lower bound for towed array shape estimation with a single source," *IEEE Trans. Signal Processing*, vol. 44, pp. 1033–1036, Apr. 1996.
[34] ——, "The partitioned eigenvector method for towed array shape estimation," *IEEE Trans. Signal Processing*, vol. 44, pp. 2273–2283, Sept. 1996.
[35] S. K. Srivastava and C. Ganapathy, "Experimental investigations on loop maneuver of underwater towed cable array system," *Ocean Eng.*, vol. 25, no. 1, pp. 85–102, Jan. 1998.
[36] J. M. Goldberg, "Joint direction-of-arrival and array-shape tracking for multiple moving targets," *IEEE J. Ocean. Eng.*, vol. 23, pp. 118–126, Apr. 1998.
[37] T. Söderström, J. Ježek , and V. Kučera, "An efficient and versatile algorithm for computing the covariance function of an ARMA process," *IEEE Trans. Signal Processing*, vol. 46, pp. 1591–1600, June 1998.
[38] N. V. Nikitakos, A. K. Leros, and S. K. Katsikas, "Towed array shape estimation using multimodel partitioning filters," *IEEE J. Ocean. Eng.*, vol. 23, no. 4, pp. 118–126, Oct. 1998.
[39] D. E. Calkins, "Metamodel-based towed system simulation," *Ocean Eng.*, vol. 26, no. 11, pp. 1183–1247, Nov. 1999.
[40] A. Jakoby, J. Goldberg, and H. Messer, "Source localization in shallow water in the presence of sensor location uncertainty," *IEEE J. Ocean. Eng.*, vol. 25, pp. 331–336, July 2000.
[41] F. Gini and R. Reggiannini, "On the use of Cramér-Rao-like bounds in the presence of random nuisance parameters," *IEEE Trans. Commun.*, vol. 48, pp. 2120–2126, Dec. 2000.

Petr Tichavský (M'98) graduated in 1987 from the Czech Technical University, Prague, Czechoslovakia. He received the Ph.D. degree in theoretical cybernetics from the Czechoslovak Academy of Sciences, Prague, in 1992.

Since that time, he has been with the Institute of Information Theory and Automation, Academy of Sciences of the Czech Republic, Prague. He is author and co-author of research papers in the areas of sinusoidal frequency/frequency-rate estimation, adaptive filtering, and tracking of time-varying signal parameters and algorithm-independent bounds on achievable performance. His recent research interests include independent component analysis and blind signal separation and signal processing for wireless communications.

Dr. Tichavský received the Fulbright grant for a ten-month fellowship at the Department of Electrical Engineering, Yale University, New Haven, CT, in 1994. In 2002, he received the Otto Wichterle Award from Academy of Sciences of the Czech Republic. Since 2002, he has served as associate editor of the IEEE SIGNAL PROCESSING LETTERS.

Kainam Thomas Wong (SM'01) received the B.S.E. (Chem. E.) degree from the University of California, Los Angeles, in 1985, the B.S.E.E. degree from the University of Colorado, Boulder, in 1987, the M.S.E.E. degree from Michigan State University, East Lansing, in 1990, and the Ph.D. degree in electrical engineering from Purdue University, West Lafayette, IN, in 1996.

He was a manufacturing engineer at the General Motors Technical Center, Warren, MI, from 1990 to 1991 and a Senior Professional Staff Member at the Johns Hopkins University Applied Physics Laboratory, Laurel, MD, from 1996 to 1998. He was an Assistant Professor with Nanyang Technological University, Singapore, in 1998 and with the Chinese University of Hong Kong from 1998 to 2001. He has been with the University of Waterloo, Waterloo, ON, Canada, since 2001. He was a contributing author of about 70 articles for the telecommunications section of the inaugural edition of the *CRC Dictionary of Pure and Applied Physics*. His research interest is signal processing for communications and sensor-array signal processing.

Dr. Wong has served on the Organizing Committees of the 2000 IEEE International Symposium on Circuits and Systems (ISCAS) and the 2004 IEEE International Conference on Acoustics, Speech, Signal Processing (ICASSP). He also serves on the Technical Program Committees of the 2002–2004 IEEE International Conference on Communications (ICC), the 2002 and 2003 IEEE Global Telecommunications Conference (GlobeCom), plus a dozen other conferences. He received the Premier's Research Excellence Award by the government of Ontario in 2003. He is listed in Marquis' *Who's Who in the World, Who's Who in America,* and *Who's Who in Science and Engineering*.